inorganics

MDPI

Article

Novel 3-Ethoxysalicylaldehyde Lanthanide Complexes Obtained by Decomposition of *Salen*-Type Ligands

Paula Mediavilla [1], Antonio Ribeiro [2], Ángel Gutiérrez [1], Santiago Herrero [1,3] and Mari Carmen Torralba [1,*]

[1] Department of Inorganic Chemistry, Complutense University of Madrid, Ciudad Universitaria, 28040 Madrid, Spain; paulmedi@ucm.es (P.M.); agalonso@ucm.es (Á.G.); sherrero@ucm.es (S.H.)
[2] Department of Organic Chemistry, Complutense University of Madrid, Ciudad Universitaria, 28040 Madrid, Spain; anribe01@ucm.es
[3] Knowledge Technology Institute, Complutense University of Madrid, Campus de Somosaguas, Pozuelo de Alarcón, 28223 Madrid, Spain
* Correspondence: torralba@ucm.es

Abstract: Three new asymmetrically coordinated lanthanide derivatives based on the bicompartmental *salen*-type ligands *N*,*N*′-bis(3-ethoxysalicylidene)propylene-1,3-diamine ($H_2EtOsalpr$) and 3-ethoxysalicylaldehyde (H*Etvain*) have been synthesized and structurally and photophysically characterized. All the compounds show dimeric structures of the general formula [Ln($H_2EtOsalpr$)(NO_3)$_2$(Etvain)]$_2$ (Ln = Nd, Eu, Dy), with each *salen*-type ligand bridging two lanthanide ions. The *Etvain* ligand comes from the $H_2EtOsalpr$ decomposition being coordinated to the corresponding lanthanide. The Nd(III) derivative shows fluorescence emission in the NIR region, but for the Eu(III) and Dy(III) compounds, only a broad band, attributed to the ligand emission, was observed.

Keywords: lanthanides; Schiff base complexes; salen; luminescence

check for updates

Academic Editor: Zhiping Zheng

Received: 19 February 2025
Revised: 7 March 2025
Accepted: 12 March 2025
Published: 19 March 2025

Citation: Mediavilla, P.; Ribeiro, A.; Gutiérrez, Á.; Herrero, S.; Torralba, M.C. Novel 3-Ethoxysalicylaldehyde Lanthanide Complexes Obtained by Decomposition of *Salen*-Type Ligands. *Inorganics* **2025**, *13*, 93. https://doi.org/10.3390/inorganics13030093

Copyright: © 2025 by the authors. Licensee MDPI, Basel, Switzerland. This article is an open access article distributed under the terms and conditions of the Creative Commons Attribution (CC BY) license (https://creativecommons.org/licenses/by/4.0/).

1. Introduction

Lanthanide(III) ions are a series of elements that exhibit a number of interesting luminescent and magnetic properties with a wide range of applications [1,2]. The photophysical properties and high quantum yields exhibited by these cations are due to electronic transitions between the 4*f* orbitals, whose emission lines span much of the electromagnetic spectrum from the UV/Vis to the infrared and can give both phosphorescence and fluorescence events. Although the luminescence of these ions makes them very promising elements for their use in the synthesis of materials with different properties, they have a drawback: *f-f* transitions are forbidden by the selection rules, which results in high quantum yields but poor luminescence in materials with lanthanides. This disadvantage can be overcome by the so-called antenna effect, which consists of the indirect excitation of a cation through the absorption of energy by the metal environment and the transfer of this energy to the lanthanide so that the choice of an environment capable of absorbing more energy and acting as an 'antenna' will result in more efficient luminescent materials [3–9]. The ligand must be able to transfer this energy to the corresponding lanthanide, usually from its triplet state (T_1), since they have longer lifetimes and a more suitable energy for transfer to the lanthanide orbitals. This implies that the ligand must have an intersystem crossing (ISC) of as high as possible and a fluorescence quantum yield of as low as possible, otherwise the transfer will not be effective.

Within of the broad group of Schiff bases, the family of *N*,*N*′-bis(salicylidene)ethylene-1,2-diamine (*salen*) derivatives are of great interest [10–12]. These ligands are easy to modify,

so it is possible to change their electronic nature, their chirality, their stability, their flexibility and the number of functional compartments in their structures [13]. In turn, these ligands possess chromophore groups capable of absorbing energy, making them an interesting choice for their use as antenna ligands in the synthesis of luminescent materials. In addition to their photophysical properties, *salen*-type ligands allow a large number of modifications in their structure, which in turn permits their coordination to a wide range of atoms ranging from transition metals to lanthanides and even small molecules as chelating ligands. Then, an enormous structural variety of complexes is possible. While the presence of nitrogen donor atoms generates a tendency toward the coordination of transition metals [14,15], the introduction of groups with oxygen atoms in specific positions allows binding to metals with larger sizes and oxophilic characters, as is the case of lanthanides [15].

For that reason, the study of complexes of trivalent lanthanide ions with *salen*-type ligands has increased in recent years in order to enhance their desirable luminescent properties. In this way, the lanthanide complexes obtained by reaction with the bicompartmental *salen*-type ligand *N*,*N*′-bis(3-methoxysalicylidene)propylene-1,3-diamine ($H_2MeOsalpr$) have been widely studied (Figure 1). These compounds show notable structural diversity and several derivatives, with different dimensionalities that have been reported. These structures include examples of monomers [16], dimers [17], tetramers [18] or coordination polymers [19]. In contrast, there are no references of lanthanide structures with the very similar ligand *N*,*N*′-bis(3-ethoxysalicylidene)propylene-1,3-diamine ($H_2EtOsalpr$). With this aim in mind, we have studied the reactions of the $H_2EtOsalpr$ ligand with several lanthanide ions with the intention of using the *salen*-type ligand as antenna complex to determine the luminescent and structural properties. This combination would yield new materials with potential uses in different fields such as medicine, biology or the lighting industry [19–21].

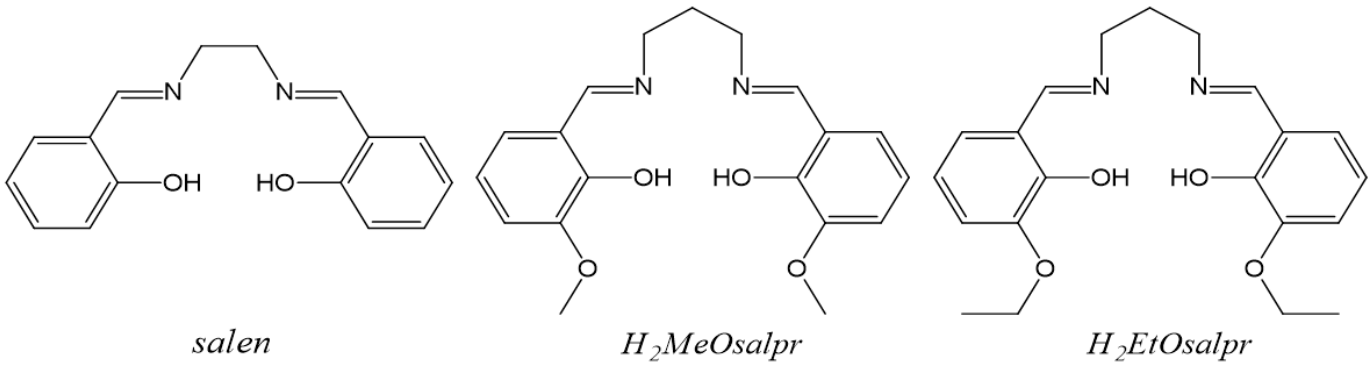


Figure 1. Salen-type ligands mentioned in the text.

2. Results and Discussion

2.1. Synthesis

New lanthanide compounds **1**–**3** (Figure 2) were synthesized by reaction between the $H_2EtOsalpr$ ligand and the corresponding lanthanide nitrate, forming a double phase and employing a methanol/acetonitrile mixture, as indicated in the experimental section. Compounds **1** and **2** were obtained as single crystals, which were suitable for single-crystal X-ray diffraction. Compound **3** precipitated as an orange powder.

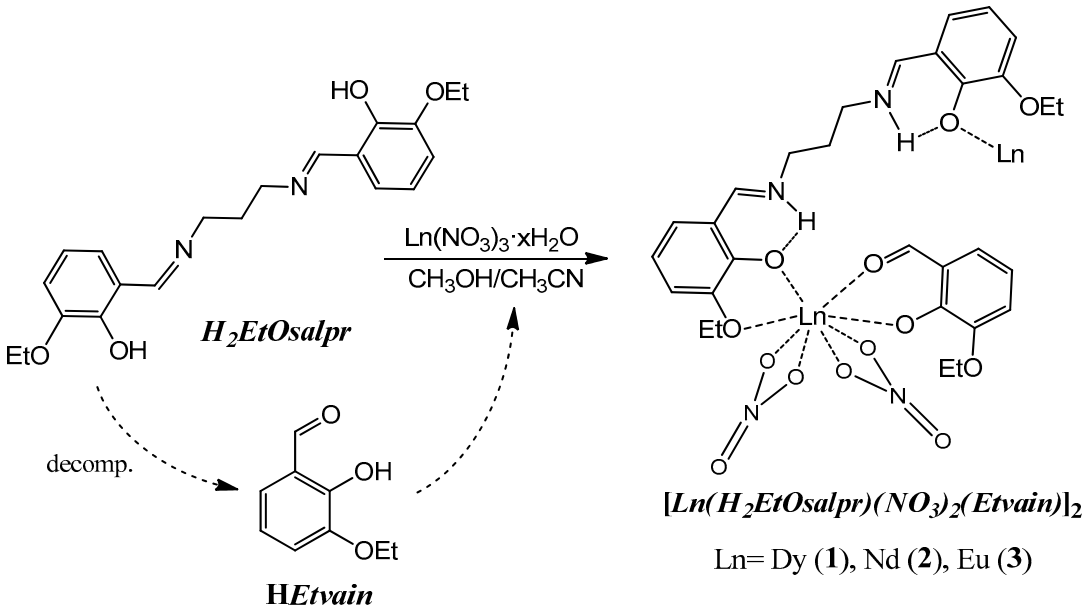


Figure 2. Scheme of the followed synthetic procedure. Only one-half of the final molecule is plotted for clarity.

All the compounds are insoluble in common organic solvents. Due to this fact, crystallization was carried out by the slow diffusion of the solutions of the respective reagents. Prolonged quiescence of the compounds resulted in the partial hydrolysis of the original ligand, giving rise to the starting reagents, the diamine and 3-ethoxysalicylaldehyde, the latter deprotonated. This process has previously been observed in Cu(II) and Fe(III) compounds coordinated to analogous *salen* derivatives [22,23]. 3-ethoxysalicylaldehyde (H*Etvain*), thus formed, can coordinate to the lanthanide ion due to the oxophilic character of these metal atoms via the carbonyl and phenoxy groups, resulting in the compounds finally obtained (Figure 2). In order to check this assumption, a reaction of dysprosium salt, the *salen*-type ligand and the 3-ethoxysalicylaldehyde in a 1:1:1 molar ration was made. The isolated compound showed the same infrared spectrum as that of compound **1**.

2.2. Infrared Spectroscopy

All the studied compounds showed similar solid-state infrared spectra, as they all have the same structure and, therefore, a minimum shift of the main bands was expected (Figure S1). Each of the spectra showed a strong band at around 1644 cm^{-1}, attributed to the ν(C=N) stretching mode of the *H_2EtOsalpr* ligand. This band shifted to higher frequencies relative to the free ligand because of its coordination to the metal ion. In the same way, the ν(C-O_{phen}) band, appearing at 1220 cm^{-1}, was moved to lower frequencies due to the coordination of the lanthanide ion to the phenolic oxygen atom. At 1619 and 1605 cm^{-1}, two additional bands were observed that corresponded to the carbonyl ν(C=O) vibration mode of the metal-coordinated *Etvain* ions. In all the complexes studied, the bands corresponding to the nitrate groups appeared at around 1440, 1300 and 1030 cm^{-1}. The values of the frequencies of the compounds obtained suggest that the nitrates were coordinated in a bidentate fashion to the metal ion [24], as confirmed by the single-crystal structure detailed below.

2.3. Single-Crystal X-Ray Diffraction Analysis

The Dy(III) complex **1** crystallized in the triclinic *P*-1 (2) space group. The molecular unit consisted of dimers of the formula [Dy(*H_2EtOsalpr*)$(NO_3)_2$(*Etvain*)]$_2$ (Figure 3), in which the Dy(III) atoms were bridged through two *H_2EtOsalpr* ligands showing a

Dy(III)···Dy(III) distance of 9.8247(5) Å. The asymmetric unit corresponded to the formula unit, since both halves of the dimer were related through an inversion center. The bridging *salen*-type ligand coordinated in a bidentate way to one of the dysprosium ions using the phenoxy and ethoxy oxygen atoms of one end, while at the other end, it was linked to the other metal ion in a monodentate fashion through the phenoxy group. The metal–oxygen bond distances were 2.246(3) and 2.283(3) Å for the phenoxy oxygen atoms and 2.714(4) Å for the weakly coordinated ethoxy group. The cation coordination was completed by the four oxygen atoms of two bidentate nitrate groups and two additional oxygen atoms corresponding to the phenoxy and carbonyl groups of a deprotonated 3-ethoxysalicylaldehyde species. The metal–oxygen bond distances in this case were 2.401(4) and 2.233(3) Å, corresponding to the carbonyl and phenoxy oxygen atoms, respectively; these distances are comparable with those found in similar compounds [25]. The coordinative environment of the dysprosium ion corresponded to nine oxygen atoms that surround the metal, forming a distortedly capped square antiprism (Figure 4).

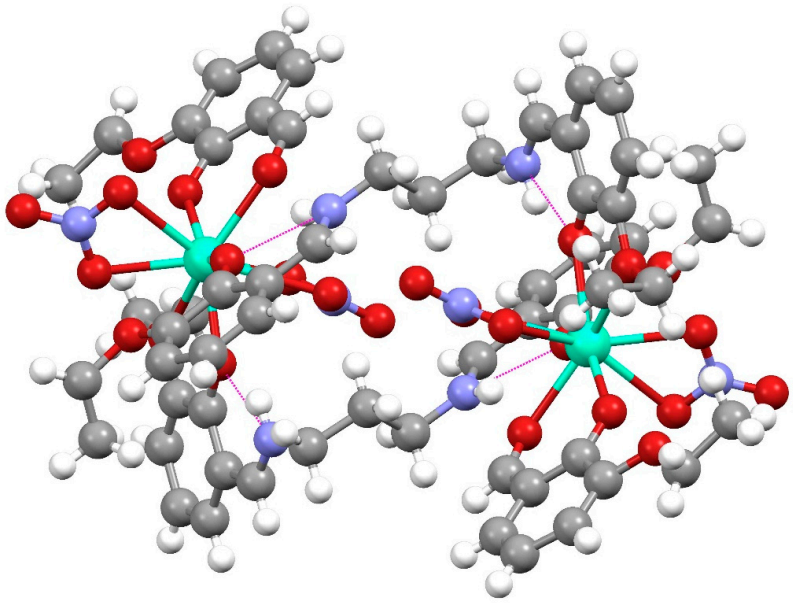


Figure 3. Dimeric unit of [Dy(H_2*EtOsalpr*)(NO_3)$_2$(*Etvain*)]$_2$ (**1**). Color code: C, grey; N, blue; O, red; H, white; Dy, cyan. Intramolecular H-bonds are plotted as magenta lines.

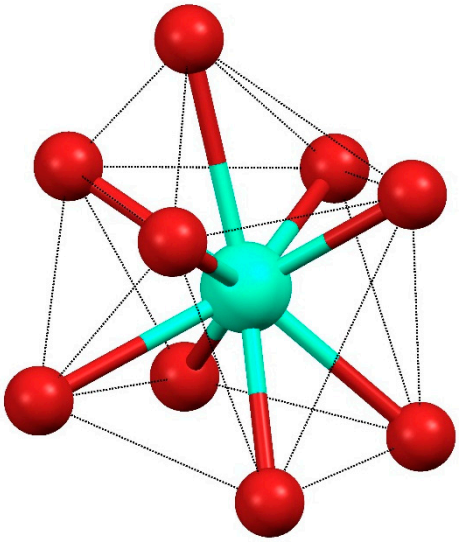


Figure 4. Coordination environment of the Dy ion in **1**.

The deprotonated 3-ethoxysalicylaldehyde species appeared in the reaction due to the cleavage of the original ligand, as has been previously commented. The *H_2EtOsalpr* ligands were neutral, with the phenolic hydrogen located on the imino nitrogen and forming an intramolecular hydrogen bond to the phenoxy oxygen atom with the distances of N-H = 0.860(5) Å and O···H = 1.988(5) Å and an N-H···O angle of 132.0(1)°. This hydrogen bond corresponded to the phenolic hydrogen migration to the imine nitrogen, as is usually observed in this type of compound [9]. The presence of this H-bond precluded any possible interactions between the lanthanide ions and the nitrogen atoms, since the Dy-N distances ranged between 4.27 and 4.5 Å, a fact expected from the oxophilicity of the lanthanide ions. The two aromatic parts of the ligand formed a torsion angle of 123.3(1)° in order to accommodate the bridge between the metal ions. Each of these dimeric units was isolated, and they did not show significant interactions between them (Figure 5).

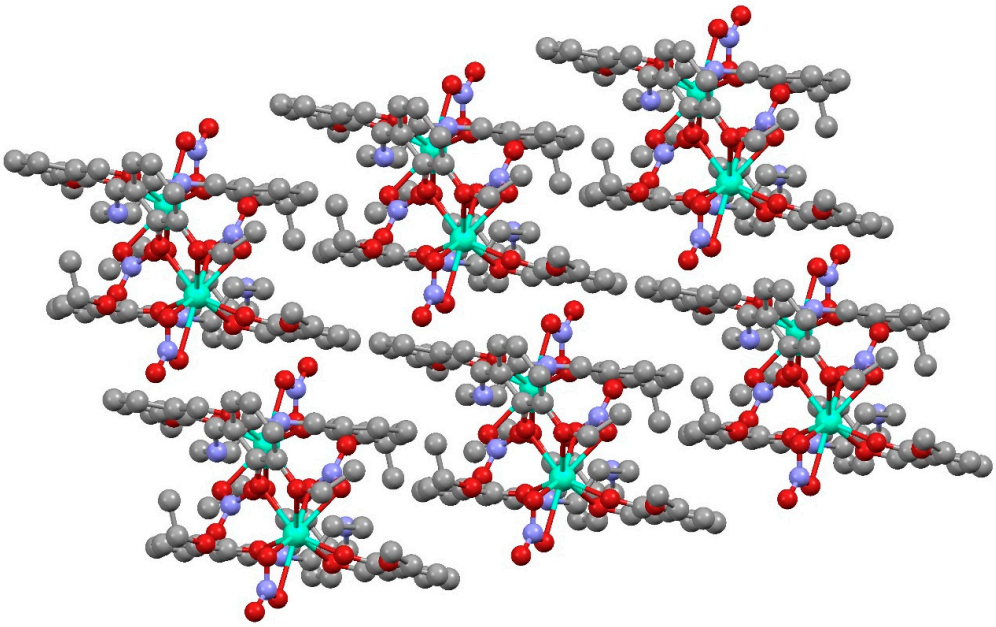


Figure 5. Packing of [Dy(*H_2EtOSalpr*)$(NO_3)_2$(*Etvain*)]$_2$ (**1**). The unit cell of the neodymium analogue, [Nd(*H_2EtOsalpr*)$(NO_3)_2$(*Etvain*)]$_2$, (**2**) was measured on a single crystal, and the obtained data indicated that it is isomorphous with the dysprosium derivative.

In a similar way, the equivalent europium complex **3** resulted in being isostructural to the Dy and Nd derivatives due to the similarity of both the infrared spectra and the powder diffraction patterns (Figure S2).

2.4. Luminescent Properties

The lanthanide compounds described in this work were expected to show emission in different spectral regions. Thus, the Nd(III) usually shows three emission bands in the NIR, centered at 880 nm, due to the fluorescence $^4F_{3/2} \rightarrow {}^4I_{9/2}$ transition, at 1060 nm ($^4F_{3/2} \rightarrow {}^4I_{11/2}$) and around 1300 nm ($^4F_{3/2} \rightarrow {}^4I_{13/2}$), the second one being much more intense than the other two. On the other hand, the Dy(III) and Eu(III) show phosphorescence phenomena. The emission of the former appears in the orange region, with a band centered at around 570 nm due to the $^4F_{9/2} \rightarrow {}^6H_{15/2 \rightarrow .\, 5/2}$ transition, while the emission of the latter appears in the red region, with a most significant maximum at 620 nm due to the $^5D_0 \rightarrow {}^7F_2$ transition.

The emission properties of the three compounds were measured in the solid state, using an excitation wavelength of 373 nm since the ligands absorbed in this region. For the emission spectra of neodymium complex **2**, a long-pass filter was always placed before detection to reduce the effects of the scattering produced by the solid. In this case, the antenna effect was

clearly observed, since an emission maximum at 1060 nm was found (Figure 6). Along with this band, a second emission at around 1340 nm can be observed, as expected.

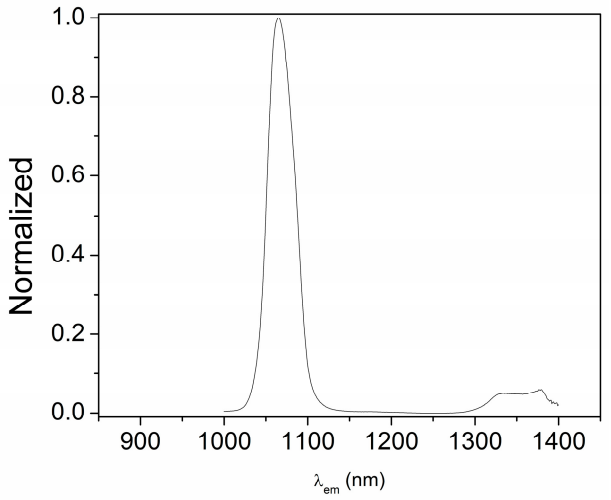


Figure 6. Emission spectra of [Nd($H_2EtOsalpr$)$(NO_3)_2$(*Etvain*)]$_2$ (**2**) in the solid state (λ_{exc} = 373 nm).

The emission spectra of the Dy and Eu complexes (**1** and **3**) showed a broad band, centered at 550 nm, that is attributed to the $H_2EtOsalpr$ ligand (see below), while the typical emission bands of the lanthanide ions were not observed (Figure 7). If we analyze these spectra, it is not clear whether the lanthanide emission occurred, since the observed band, due to the ligand, is very broad. However, the values of the half-life times for the lanthanide ions appeared in the expected range. Since these measurements are more sensitive than the emission intensities, we assumed that the lanthanide luminescence promoted by the antenna effect of the *salen*-type ligand was overlapped by the ligand emission. This fact prevents us from identifying the emission of the lanthanide ions, in contrast to what has been reported for the luminescence studies of europium and dysprosium complexes with analogous ligands [26,27].

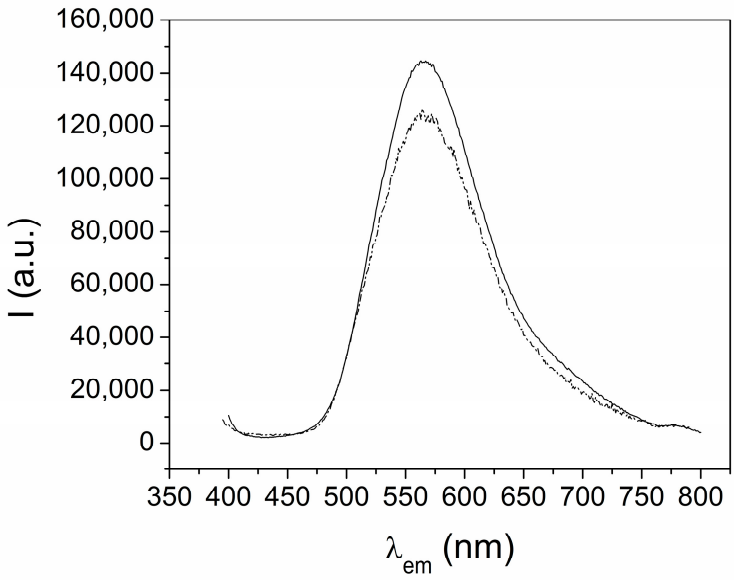


Figure 7. Emission spectra of [Dy($H_2EtOsalpr$)$(NO_3)_2$(*Etvain*)]$_2$ (**1**) (solid line) and [Eu($H_2EtOsalpr$)$(NO_3)_2$(*Etvain*)]$_2$ (**3**) (dashed line) in the solid state (λ_{exc} = 373 nm).

The presence of the broad emission band at 550 nm led us to study the luminescent properties of the ligands involved: in particular, H_2*EtOsalpr*, which, in theory, is a ligand able to allow an energy transfer to the corresponding lanthanide ion.

The absorption and emission spectra of the H_2*EtOsalpr* ligand are shown in Figure 8. The ligand absorbs in the UV region and emits in the visible. The absorption spectrum shows typical bands at 224, 262 and 334 nm, corresponding, respectively, to the transitions $\sigma \rightarrow \sigma^*$, $\pi \rightarrow \pi^*$ and $n \rightarrow \pi^*$.

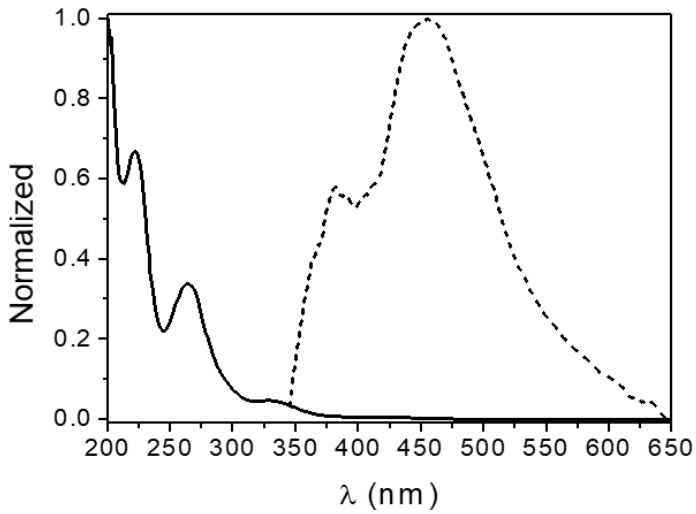


Figure 8. Normalized absorption (solid line) and emission spectra (dashed line, λ_{exc} = 330 nm) of the H_2*EtOsalpr* ligand in acetonitrile solution.

The cut-off point between the excitation (or absorption) spectra and the emission spectra gives information about the bandgap between the S_1 and S_0 states. In this case, the bandgap of the H_2*EtOsalpr* ligand in acetonitrile was 3.60 eV (345 nm).

Figure 9 shows the excitation and emission spectra of an ethanol solution of the H_2*EtOsalpr* and H*Etvain* species. As can be observed, both ligands absorbed and emitted in similar regions, a fact that could be detrimental to the transfer process to the lanthanide ion, as it would be difficult to selectively excite only the H_2*EtOsalpr* ligand, which is the ligand responsible for the antenna effect.

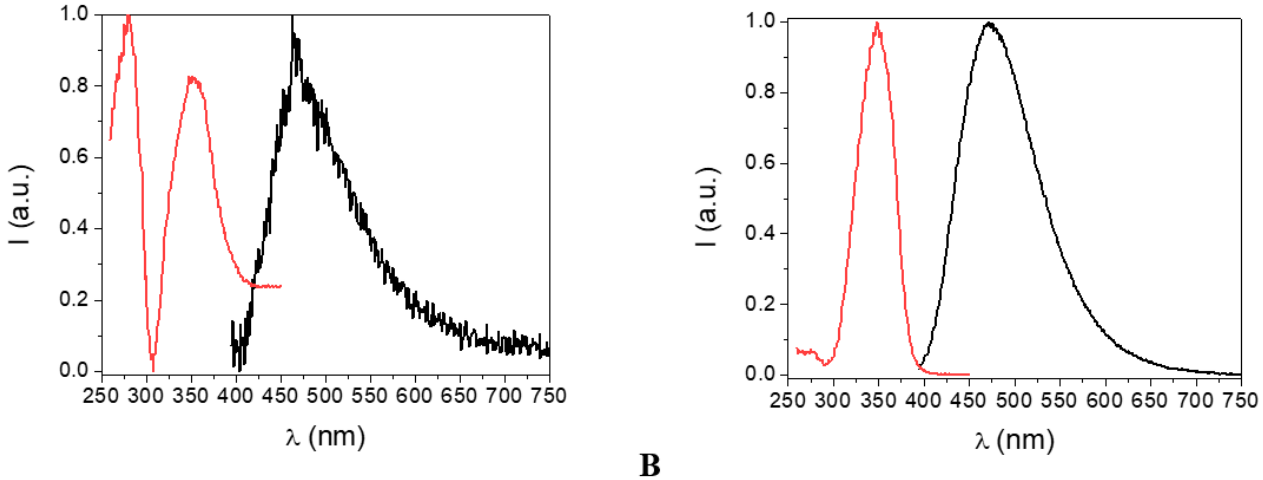


Figure 9. Normalized excitation (red) and emission (black) spectra of the H_2*EtOsalpr* (**A**) and H*Etvain* (**B**) species in ethanol at 298 K. In both cases, λ_{exc} = 330 nm for the emission spectra. For the excitation spectra, λ_{em} = 473 nm for H_2*EtOsalpr* and λ_{em} = 479 nm for H*Etvain*.

It should be noted that the *H_2EtOsalpr* ligand in the polar solvents favored the charge transfer state and also stabilized the transitions of $\pi \rightarrow \pi^*$ and $n \rightarrow \pi^*$; hence, the cut-off point between the excitation and emission spectra was shifted to 418 nm (2.97 eV). This value is lower than expected for the bandgap between the S_1 and S_0 states and more probably corresponds to a charge transfer state into the ligand. In the H*Etvain* case, the bandgap was approximately 396 nm (3.14 eV).

The fluorescence lifetimes of the *H_2EtOsalpr* and H*Etvain* species were also measured (Figure S3 and Table S1). These lifetimes are typical for fluorescence, and there was a slightly longer one for the *H_2EtOsalpr* ligand. The $^1O_2$ production of the *H_2EtOsalpr* ligand was measured in order to estimate the intersystem crossing (ISC). This value can give us information on how much the T_1 level was populated, but no $^1O_2$ has been observed (Figure S4). This result may indicate either that there was no production of $^1O_2$ or that the quantum yield of the ISC was very low.

Figure 10 shows the emission spectra of the *H_2EtOsalpr* ligand at 77 K collected at different time scales. The steady-state emission spectrum shows a high overlap of fluorescence and phosphorescence. Collecting the spectra at different time scales, it was possible to separate the fluorescence and phosphorescence emissions. The fluorescence maximum appeared at 516 nm (2.41 eV), while the phosphorescence maximum was observed at 544 nm. The triplet energy was estimated at the wavelength where the intensity was 10% with respect to the phosphorescence maximum value. Since this maximum appeared at 544 nm (2.29 eV), we can estimate the triplet energy at around 467 nm (2.68 eV).

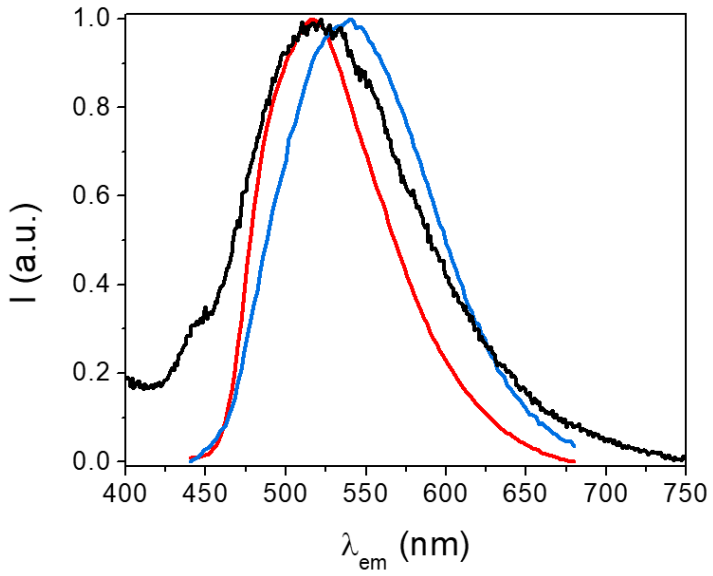


Figure 10. Stationary emission spectra (black) and at different time scales: emissions lasting between 0.1 and 0.2 μs (red, fluorescence) and between 1 and 2 μs (blue, phosphorescence). All spectra have been measured at 77 K (λ_{exc} = 373 nm).

At 77 K, the lifetime was estimated at the emission maximum (Table 1 and Figure S4).

Table 1. Fluorescence lifetimes of *H_2EtOsalpr* in ethanol at 298 K (λ_{exc} = 373 and λ_{em} = 479 nm) and emission lifetimes of *H_2EtOsalpr* in ethanol at 77 K (λ_{exc} = 373 and λ_{em} = 518 nm).

t (ns)	λ_{em} = 479 nm, 298 K	λ_{em} = 518 nm, 77 K Fluorescence Lifetimes	λ_{em} = 518 nm, 77 K Phosphorescence Lifetimes
τ_1	6.2	4.9	3090
τ_2	2.4	1.8	363
τ_{int}	4.0	3.4	2200
τ_{amp}	3.3	2.7	900

At 77 K, we were able to observe both fluorescence and phosphorescence and determine their corresponding lifetimes, and we have been able to determine the energy of T_1 in ethanol. In principle, the T_1 energy of the ligand is sufficient to produce fluorescence on the neodymium(III) ion and phosphorescence both in the dysprosium(III) and europium(III) ions, but with a low ligand ISC, this transfer will not occur efficiently.

3. Materials and Methods

3.1. Materials

The synthesis of these compounds was carried out using products and solvents from Sigma-Aldrich (Diegem, Belgium) and ThermoScientific (Waltham, MA, USA). The preparation of the ligand *N*,*N*′-bis(3-ethoxysalicylidene)propylene-1,3-diamine (*H*$_2$*EtOsalpr*) was carried out by a reaction between propylenediamine and 3-ethoxysalicylaldehyde (H*Etvain*) according to the literature [14,28].

3.2. Physical Measurements

The infrared spectra were collected in the solid state using a Fourier transform spectrophotometer with the ATR Perkin-Elmer accessory Spectrum 100 in the range of 4000–550 cm^{-1} with a 4 cm^{-1} resolution (UCM, Madrid, Spain). The CHN elemental analysis was performed on a LECO CHNS-932 at the Microanalysis Unit of the UCM (Madrid, Spain). Single-crystal data for [Dy(*H*$_2$*EtOsalpr*)(NO$_3$)$_2$(*Etvain*)]$_2$ (**1**) were collected at room temperature on a Bruker APEX-II CCD diffractometer working with graphite monochromated Cu-K$_{alpha}$ radiation (λ = 1.54184 Å) at the X-ray Diffraction Unit of the UCM (Madrid, Spain). The cell parameters were determined and refined by the least-squares fit of all the reflections collected, and a semiempirical absorption correction was applied to the reduced data using the SADABS program [29]. The structures were solved by intrinsic phasing using the SHELXT solution program [30] and refined by full-matrix least-squares on F^2 using the SHEXL refinement package [31] running in the Olex2 environment [32]. All non-hydrogen atoms were refined anisotropically. The hydrogen atoms were included with fixed isotropic contributions at their calculated positions determined by molecular geometry. The methyl carbon atoms were modelized as disordered between two alternate positions, with fixed occupancy factors of 0.5. The ultimate-difference Fourier maps revealed no peaks of chemical significance. Information on the data collection parameters, crystallographic data and final agreement parameters appears in Table 2. The CCDC deposit number for compound **1** is 2395092. X-ray powder diffraction (XRPD) measurements were performed in a Bruker D8 Advance diffractometer with monochromatized CuKα radiation. Simulated XRPD patterns from the single-crystal data were obtained with the Mercury 4.0 software [33].

The absorption, emission and emission lifetime spectra of all the studied substances were measured in HPLC-grade acetonitrile solutions using quartz cells with a 1 cm optical path length. The UV/Vis absorption spectra were recorded on a single-beam Varian Cary 50 spectrophotometer (UCM, Madrid, Spain). The fluorescence, excitation and phosphorescence spectra were recorded using a FluoTime 300 time-correlated single-photon-counting (TCSPC) spectrofluorometer (PicoQuant) equipped with a 300 W Xe-lamp as a steady-state excitation system with a spectral range from 250 nm to 2600 nm and a Peltier cooled photomultiplier tube (PMT, PMA-C 192-M type, 230–920 nm) (UCM, Madrid, Spain). The emission lifetimes were determined using, as an excitation source, a diode laser head emitting at 373 nm (LDH-P-C-375, temperature-stabilized laser emitting collimated picosecond pulses), and the emitted photons were detected, keeping the count rate below 1% to avoid artifacts such as the pile-up effect (PMA-C 192-M PMT and TimeHarp 260 PICO Single TCSPC PC plugin board for independent PCIe bus channels with 25 ps time resolution).

The solid-emission measurements were performed by introducing a fine powder of the compound between two glass coverslips.

Table 2. Crystal data and structure refinement for compound **1**.

Empirical Formula	$\mathbf{C_{60}H_{66}Dy_2N_8O_{26}}$
Formula weight	1640.2
Temperature	293(2) K
Wavelength	1.54184 Å
Crystal system	Triclinic
Space group	*P*–1 (2)
Unit cell dimensions	a = 10.1607(3) Å b = 10.6719(3) Å c = 17.0363(5) Å α = 74.543(2)° β = 79.487(2)° γ = 80.239(2)°
Volume	1736.30(9) $Å^3$
Z	1
Crystal size	0.11 × 0.08 × 0.02 mm
Density(calculated)	1.569 g/cm^3
μ	12.102 mm^{-1}
Theta(max)	68.31°
Goodness-of-fit on F^2	0.994
Refinement	$R[F^2 > 2\sigma(F^2)] = 0.0471$ $wR(F^2) = 0.1255$
Rint	0.18
Largest diff. peak and hole	1.644, −0.878 eA^{-3}

As the T_1 of the ligands was involved in the antenna effect, all measurements in the solutions were performed by purging with Ar for at least 15 min, since the atmospheric oxygen was a fluorescence quencher, but above all, it was very effective in quenching the T_1 state and, thus, phosphorescence.

The emission spectra and emission lifetimes under an inert atmosphere were measured with solvent-saturated Ar-purged solutions. The fluorescence and phosphorescence measurements of the *H_2EtOsalpr* ligand at 77 K were performed in HPLC-grade ethanol.

The $^1O_2$ production was determined by directly detecting the lifetime of the $^1O_2$ phosphorescence using the 373 nm laser, measuring at 1270 nm and using an 850 nm long-pass filter to eliminate the possible harmonics of the emission and excitation.

The EasyTau 2 program was used to acquire the emission and excitation spectra and to measure the emission lifetimes, and the extension of this program, Fluofit, was used to obtain the emission lifetimes.

3.3. Synthesis of the Compounds

All the compounds obtained were synthesized using the same method. As an example, the synthesis of the dysprosium derivative is described:

[Dy(H_2EtOsalpr)(NO_3)$_2$(Etvain)]$_2$ (**1**): A solution of 0.225 g (0.61 mmol) of the ligand *H_2EtOSalpr* in 8 mL of acetonitrile was placed in a test tube. Over this solution, 0.224 g (0.61 mmol) of $Dy(NO_3)_3 \cdot H_2O$ dissolved in 8 mL of methanol was slowly added to obtain a double layer, which was kept at rest. After several days, single crystals suitable for X-ray diffraction were obtained. Analysis calculated for $C_{30}H_{35}DyN_4O_{13}$: C 43.83; H 4.29; N 6.81%. Found C, 43.77; H, 4.41; N, 6.81%. Most significant IR bands (cm^{-1}): 1644, 1618, 1605 ν(C=N) and ν(C=O); 1215 $\nu(C\text{-}O)_{phen}$ and 1053 ν_s(C-OEt); 1456 ν(N=O); 1297 $\nu_{as}(NO_2)$; 1032 $\nu_s(NO_2)$.

[Nd(H_2EtOsalpr)(NO_3)$_2$(Etvain)]$_2$ (**2**): Analysis calculated for $C_{30}H_{35}NdN_4O_{13}$: C 44.82; H 4.39; N 6.97%. Found C, 44.08; H, 4.36; N, 7.13%. Most significant IR bands (cm^{-1}): 1642, 1619, 1606 ν(C=N) and ν(C=O); 1218 $\nu(C\text{-}O)_{phen}$; 1071 ν_s(C-OEt); 1440 ν(N=O); 1299 $\nu_{as}(NO_2)$; 1032 $\nu_s(NO_2)$.

[Eu(H_2EtOsalpr)(NO_3)$_2$(Etvain)]$_2$ (**3**): Analysis calculated for $C_{30}H_{35}EuN_4O_{13}$: C, 44.40; H, 4.35; N, 6.90%; C, 43.67; H, 4.31; N, 6.98%. Significant IR bands (cm^{-1}) 1644, 1618, 1605 ν(C=N) and ν(C=O); 1219 $\nu(C\text{-}O)_{phen}$; 1075 ν_s(C-OEt); 1442 ν(N=O); 1306 $\nu_{as}(NO_2)$; 1032 $\nu_s(NO_2)$.

Dysprosium compound **1** was also synthesized by an alternate method: A solution of 0.225 g (0.61 mmol) of the ligand *H_2EtOsalpr* and 0.101 g (0.61 mmol) of H*Etvain* in 10 mL of acetonitrile was stirred in a round-bottom flask. Over this solution, 0.224 g (0.61 mmol) of $Dy(NO_3)_3{\cdot}H_2O$ dissolved in 5 mL of methanol were added. After two hours of stirring, a yellow solid precipitated. The solid was filtered, washed with methanol and vacuum-dried. The yield was 67%.

4. Conclusions

The reaction of *N*,*N*′-bis(3-ethoxysalicylidene)propylene-1,3-diamine (*H_2EtOsalpr*) with nitrate salts of dysprosium, neodymium and europium took place with the partial hydrolysis of *salen*-type ligands and coordination of deprotonated 3-ethoxysalicylaldehyde (*Etvain*) to the lanthanide ion. The final obtained derivatives were dimers with the metal ions bridged by two asymmetrically coordinated *H_2EtOsalpr* ligands. The luminescent properties of these compounds are clearly dominated by the emission of the *salen*-type ligand that presents the singlet and triplet excited states very closely in energy. This fact can favor the thermally activated delayed fluorescence of the ligand in detriment of its antenna effect and, therefore, restrains the energy transfer to the lanthanide ions. For this reason, no neat emissions were observed for the dysprosium and europium compounds, whose phosphorescence signal should have overlapped with the more intense ligand emission. On the contrary, the neodymium ion presented a neat fluorescence emission signal in the NIR region, distant enough from the ligand emission, making this compound a good candidate for use in medical applications due to the usual biocompatibility observed in *salen* ligands [34,35].

Supplementary Materials: The following supporting information can be downloaded at: https://www.mdpi.com/article/10.3390/inorganics13030093/s1, Figure S1: Superposition of the IR spectra in solid state of the obtained compounds: **1** (Dy) black line, **2** (Nd) green line, **3** (Eu) red line; Figure S2: Superposition of the powder X-ray diffractograms of the obtained compounds: **1** (Dy) black line, **2** (Nd) green line, **3** (Eu) red line; Figure S3: Fluorescence lifetimes of *H_2EtOSalpr* (red) and H*Etvain* (black) in ethanol at 298 K (λ_{exc} = 373 y λ_{em} = 479 nm); Figure S4: Phosphorescence lifetime of $^1O_2$ in ethanol at 298 K (λ_{exc} = 373 nm and λ_{em} = 1270 nm); Figure S5: Fluorescence lifetimes of *H_2EtOSalpr* in ethanol at 298 K (black, λ_{exc} = 373 and λ_{em} = 479 nm) and emission lifetimes of *H_2EtOSalpr* in ethanol at 77 K (red, λ_{exc} = 373 and λ_{em} = 518 nm); Figure S6: Phosphorescence lifetimes of *H_2EtOSalpr* in ethanol at 77 K (λ_{exc} = 373 and λ_{em} = 518 nm); Figure S7: Emission spectra and luminescence lifetimes for the Dy derivative (**1**) in solid state; Figure S8: Emission spectra and luminescence lifetimes for the Nd derivative (**2**) in solid state; Figure S9: Emission spectra and luminescence lifetimes for the Eu derivative (**3**) in solid state; Table S1: Fluorescence lifetimes of *H_2EtOSalpr* (red) and *Etvain* (black) in ethanol at 298 K (λ_{exc} = 373 y λ_{em} = 479 nm); Table S1: Fluorescence lifetimes of H_2EtOSalpr (red) and Etvain (black) in ethanol at 298 K (λ_{exc} = 373 y λ_{em} = 479 nm).

Author Contributions: Conceptualization, M.C.T. and Á.G.; methodology, P.M., M.C.T. and Á.G.; software, A.R. and Á.G.; validation, P.M., A.R. and S.H.; investigation, P.M. and A.R.; resources, P.M. and A.R.; writing—original draft preparation, P.M. and A.R.; writing—review and editing, M.C.T., Á.G. and S.H.; supervision, M.C.T. and Á.G.; project administration, M.C.T. and S.H.; funding acquisition, M.C.T. and S.H. All authors have read and agreed to the published version of the manuscript.

Funding: The authors gratefully acknowledge financial support from the Complutense University of Madrid, ref. PR3/23-30828, and the Community of Madrid, ref. TEC-2024/TEC-85. One of us (P.M.) thanks the Science Ministry for one INVESTIGO contract, ref. CT19-23-INVM-48-20230426-120332. One of us (A.R.) thanks the CAM and the European Union for funding this project with reference REACT ANTICIPA-UCM (SP6) and the Ministry of Science, Innovation and Universities for funding the project with reference number PID2020-114653RB-I00/AEI/10.13039/501100011033, 'Synthesis and applications of carbon nanostructures with unconventional properties', and the project with reference number FEI-EU-20-09, 'Synthesis "Botton-Up" of carbon nanostructures: applications for energy'.

Data Availability Statement: The original contributions presented in this study are included in the article and Supplementary Materials. Further inquiries can be directed to the corresponding author.

Conflicts of Interest: The authors declare no conflicts of interest.

References

1. Bünzli, J.-C.G.; Piguet, C. Taking advantage of luminescent lanthanide ions. *Chem. Soc. Rev.* **2005**, *34*, 1048–1077. [CrossRef] [PubMed]
2. Wang, M. Current Development of Lanthanide Complexes for Biomedical Applications. *Chem. Asian J.* **2024**, *19*, e202400038. [CrossRef] [PubMed]
3. Tang, M.J.; Zhu, Z.H.; Li, Y.L.; Qin, W.W.; Liang, F.P.; Wang, H.L.; Zou, H.H. Specific smart sensing of electron-rich antibiotics or histidine improves the antenna effect, luminescence, and photodynamic sterilization capabilities of lanthanide polyoxometalates. *J. Colloid Interface Sci.* **2025**, *680*, 235–246. [CrossRef] [PubMed]
4. Eliseeva, S.V.; Bünzli, J.-C.G. Lanthanide luminescence for functional materials and bio-sciences. *Chem. Soc. Rev.* **2010**, *39*, 189–227. [CrossRef]
5. Bünzli, J.-C.G. On the design of highly luminescent lanthanide complexes. *Coord. Chem. Rev.* **2015**, *293–294*, 19–47. [CrossRef]
6. Martinon, T.L.M.; Pierre, V.C. Luminescent lanthanide probes for cations and anions: Promises, compromises, and caveats. *Curr. Opin. Chem. Biol.* **2023**, *76*, 102374. [CrossRef]
7. Hasegawa, M.; Ohmagari, H.; Tanaka, H.; Machida, K. Luminescence of lanthanide complexes: From fundamental to prospective approaches related to water- and molecular-stimuli. *J. Photochem. Photobiol. C* **2022**, *50*, 100484. [CrossRef]
8. Badiane, A.M.; Freslon, S.; Daiguebonne, C.; Suffren, Y.; Bernot, K.; Calvez, G.; Costuas, K.; Camara, M.; Guillou, O. Lanthanide-Based Coordination Polymers with a 4,5-Dichlorophthalate Ligand Exhibiting Highly Tunable Luminescence: Toward Luminescent Bar Codes. *Inorg. Chem.* **2018**, *57*, 3399–3410. [CrossRef]
9. Godoy-Alcántar, C.; Yatsimirsky, A.K.; Lehn, J.M. Structure-stability correlations for imine formation in aqueous solution. *J. Phys. Org. Chem.* **2005**, *18*, 979–985. [CrossRef]
10. Boulechfar, C.; Ferkous, H.; Delimi, A.; Djedouani, A.; Kahlouche, A.; Boublia, A.; Darwish, A.S.; Lemaoui, T.; Verma, R.; Benguerba, Y. Schiff bases and their metal Complexes: A review on the history, synthesis, and applications. *Inorg. Chem. Commun.* **2023**, *150*, 110451. [CrossRef]
11. Zhang, J.; Xu, L.; Wong, W.-Y. Energy materials based on metal Schiff base complexes. *Coord. Chem. Rev.* **2018**, *355*, 180–198. [CrossRef]
12. Abu-Dief, M.A.; Mohamed, I.M.A. A review on versatile applications of transition metal complexes incorporating Schiff bases. *Beni-Suef Univ. J. Basic Appl. Sci.* **2015**, *4*, 119–133. [CrossRef] [PubMed]
13. Nworie, F.S. Bis(salicylidene)ethylendiamine (salen) and bis(salycilene)ethilenediamine-metal complexes from structure to biological activity. *J. Anal. Pharm. Res.* **2016**, *3*, 76–85. [CrossRef]
14. Al-Obaidi, F.N.; Al-Diwan, T.A.; Mahdi, A.S. Study of the Coordination Tendency of [N,N′-Ethylenebis(salicylidenimine)] Towards Transition Metal Ions. *Int. J. Pure Appl. Chem.* **2010**, *52*, 131–134.
15. Azam, M.; Al-Resayes, S.I. Phenoxy-bridged binuclear Zn(II) complex holding salen ligand: Synthesis and structural characterization. *J. Mol. Struct.* **2016**, *1107*, 77–81. [CrossRef]
16. Gao, T.; Li, G.M.; Gao, P.; Yan, P.F.; Hou, G.F. [*N*,*N*′-Bis(3-methoxy-2-oxidobenzylidene)ethane-1,2-diaminium-κ^4*O*,*O*′,*O*″,*O*‴]tris(nitrato-κ^2*O*,*O*′)erbium(III). *Acta Crystallogr. E* **2010**, *66*, m107. [CrossRef]
17. Wang, J.H.; Yan, P.F.; Li, G.M.; Zhang, J.W.; Chen, P.; Suda, M.; Einaga, Y. *N*,*N*′-bis(2-hydroxy-3-methoxybenzylidene)-1,3-diaminopropane dimeric 4f and 3d-4f heterodinuclear complexes: Syntheses, crystal structures and magnetic properties. *Inorg. Chim. Acta* **2010**, *363*, 3706–3713. [CrossRef]
18. Wu, J.; Li, X.-L.; Zhao, L.; Guo, M.; Tang, J. Enhancement of Magnetocaloric Effect through Fixation of Carbon Dioxide: Molecular Assembly from Ln_4 to Ln_4 Cluster Pairs. *Inorg. Chem.* **2017**, *56*, 4104–4111. [CrossRef]

19. Kaczmarek, A.M.; Porebski, P.W.A.; Mortier, T.; Lynen, F.; Van Deun, R.; Van Hecke, K. Near-infrared luminescence and RNA cleavage ability of lanthanide Schiff base complexes derived from *N*,*N*′-bis(3-methoxysalicylidene)ethylene-1,2-diamine ligands. *J. Inorg. Biochem.* **2016**, *163*, 194–205. [CrossRef]
20. Debroye, E.; Parac-Vogt, T.N. Towards polymetallic lanthanide complexes as dual contrast agents for magnetic resonance and optical imaging. *Chem. Soc. Rev.* **2014**, *43*, 8178–8192. [CrossRef]
21. Andruh, M. The exceptionally rich coordination chemistry generated by Schiff-base ligands derived from *o*-vanillin. *Dalton Trans.* **2015**, *44*, 16633–16653. [CrossRef] [PubMed]
22. Nayak, M.; Sarkar, S.; Lemoine, P.; Sasmal, S.; Koner, R.; Sparkes, H.A.; Howard, J.A.K.; Mohanta, S. Supramolecular Dimers of Copper(II) Complexes Resulting from Designed Host–Guest Interactions. *Eur. J. Inorg. Chem.* **2010**, *2010*, 744–752. [CrossRef]
23. Ramadan, R.M.; Abu Al-Nasr, A.K. Unusual Catalytic Process Involving OH and NH Exchange. *Int. J. Org. Chem.* **2012**, *2*, 64–70. [CrossRef]
24. Nakamoto, K.; Czernuszewicz, R.S. Infrared Spectroscopy. *Methods Enzymol.* **1993**, *226*, 259–289. [CrossRef]
25. Shi, D.; Yang, X.; Ma, Y.; Niua, M.; Jones, R.A. Construction of 14-metal lanthanide nanorings with NIR luminescence response to ions. *Chem. Commun.* **2020**, *56*, 8651. [CrossRef]
26. Lozovan, V.; Borodi, G.; Perhat, I.; Turza, A.; Branzanic, A.M.V.; Pîrnau, A.; Mures, L.E. EuIII complexes derived from 2-quinolinecarbohydrazide Schiff base ligand, relations between structure and luminescence properties. *J. Mol. Struct.* **2025**, *1322*, 140397. [CrossRef]
27. Cristóvão, B.; Hnatejko, Z. LanthanideIII compounds with the N_2O_4-donor Schiff base—Synthesis, spectral, thermal, magnetic and luminescence properties. *J. Mol. Struct.* **2015**, *1088*, 50–55. [CrossRef]
28. Contreras, R.; Rojas Pérez, Y. Salen's ligands in coordination chemistry. A short review. *Cienc. Ing.* **2018**, *39*, 307–314.
29. Sheldrick, G.M. *SADABS, Version 2.05. A Software for Empirical Absorption Correction*; University of Göttingen: Göttingen, Germany, 2002.
30. Sheldrick, G.M. SHELXT—Integrated space-group and crystal-structure determination. *Acta Crystallogr. A* **2015**, *71*, 3–8. [CrossRef]
31. Sheldrick, G.M. Crystal structure refinement with SHELXL. *Acta Crystallogr. C* **2015**, *71*, 3–8. [CrossRef]
32. Dolomanov, O.V.; Bourhis, L.J.; Gildea, R.J.; Howard, J.A.K.; Puschmann, H. OLEX2: A complete structure solution, refinement and analysis program. *J. Appl. Crystallogr.* **2009**, *42*, 339–341. [CrossRef]
33. Macrae, C.F.; Sovago, I.; Cottrell, S.J.; Galek, P.T.A.; McCabe, P.; Pidcock, E.; Platings, M.; Shields, G.P.; Stevens, J.S.; Towler, M.; et al. Mercury 4.0: From visualization to analysis, design and prediction. *J. Appl. Crystallogr.* **2020**, *53*, 226–235. [CrossRef] [PubMed]
34. Nidhi; Siddharam; Rao, D.P.; Gautam, A.K.; Verma, A.; Gautam, Y. Schiff bases and their possible therapeutic applications: A review. *Results Chem.* **2025**, *13*, 101941. [CrossRef]
35. More, M.S.; Joshi, P.G.; Mishra, Y.K.; Khanna, P.K. Metal complexes driven from Schiff bases and semicarbazones for biomedical and allied applications: A review. *Mater. Today Chem.* **2019**, *14*, 100195. [CrossRef]

Disclaimer/Publisher's Note: The statements, opinions and data contained in all publications are solely those of the individual author(s) and contributor(s) and not of MDPI and/or the editor(s). MDPI and/or the editor(s) disclaim responsibility for any injury to people or property resulting from any ideas, methods, instructions or products referred to in the content.